Research Article | Vol. 25, No. 23 | 13 Nov 2017 | OPTICS EXPRESS 28946
Optics EXPRESS

Non-traditional whispering gallery modes inside microspheres visualized with Fourier analysis

LANTIAN CHANG,* FRANK TIMMERMANS, AND CEES OTTO

Medical Cell BioPhysics Group, MIRA Institute, University of Twente, P.O. Box 217, 7500 AE Enschede, The Netherlands
**l.chang@utwente.nl*

Abstract: Non-traditional whispering gallery modes are studied in a glass microsphere. Geometrical ray tracing is used to explain and calculate these modes. Thermal emission and Raman scattering are used as an internal light source to excite these modes inside the glass microsphere. The thermal and Raman emission spectra are modified due to the existence of these modes. Fourier analysis is then used to distinguish the individual modes. The understanding of these non-traditional WGM may lead to alternative design strategies for sensor applications or laser cavity configurations.

OCIS codes: (030.4070) Modes; (080.0080) Geometric optics; (300.6300) Spectroscopy; (070.0070) Fourier optics and signal processing; (230.5750) Resonators; (180.5655) Raman microscopy.

References and links

1. M. R. Foreman, J. D. Swaim, and F. Vollmer, "Whispering gallery mode sensors," Adv. Opt. Photonics **7**(2), 168–240 (2015).
2. A. Bozzola, S. Perotto, and F. De Angelis, "Hybrid plasmonic-photonic whispering gallery mode resonators for sensing: a critical review," Analyst (Lond.) **142**(6), 883–898 (2017).
3. M. Humar and S. H. Yun, "Intracellular microlasers," Nat. Photonics **9**, 572 (2015).
4. T. Kumagai, T. Kishi, and T. Yano, "Low threshold lasing of bubble-containing glass microspheres by non-whispering gallery mode excitation over a wide wavelength range," J. Appl. Phys. **117**, 113104 (2015).
5. V. B. Braginsky, M. L. Gorodetsky, and V. S. Ilchenko, "Quality-Factor and Nonlinear Properties of Optical Whispering-Gallery Modes," Phys. Lett. A **137**, 393–397 (1989).
6. J. B. Keller, "Asymptotic Solution of Eigenvalue Problems," Ann. Phys. **9**, 24–75 (1960).
7. G. Roll and G. Schweiger, "Geometrical optics model of Mie resonances," J. Opt. Soc. Am. A **17**(7), 1301–1311 (2000).
8. L. G. Guimaraes and H. M. Nussenzveig, "Theory of Mie Resonances and Ripple Fluctuations," Opt. Commun. **89**, 363–369 (1992).
9. M. L. Gorodetsky and A. E. Fomin, "Geometrical theory of whispering-gallery modes," Ieee J. Sel. Top. Quant. **12**, 33–39 (2006).
10. G. Roll, T. Kaiser, S. Lange, and G. Schweiger, "Ray interpretation of multipole fields in spherical dielectric cavities," J. Opt. Soc. Am. A **15**, 2879–2891 (1998).
11. D. Q. Chowdhury, D. H. Leach, and R. K. Chang, "Effect of the Goos-Hanchen Shift on the Geometrical-Optics Model for Spherical-Cavity Mode Spacing," J. Opt. Soc. Am. A **11**, 1110–1116 (1994).
12. R. C. Gauthier, "Whispering-gallery modes of mu-optic silicon bottle resonator examined using a Fourier-Bessel eigen-state approach," J. Micro-Nanolith. Mem. **12**, 043007 (2013).
13. T. Ioppolo, N. Das, and M. V. Otugen, "Whispering gallery modes of microspheres in the presence of a changing surrounding medium: A new ray-tracing analysis and sensor experiment," J. Appl. Phys. **107**, 103105 (2010).
14. L. Chang, *Chip Based Common-path Swept-source Optical Coherence Tomography Device* (Universiteit Twente, 2016).
15. F. J. Timmermans, L. Chang, H. A. G. M. van Wolferen, A. T. M. Lenferink, and C. Otto, "Observation of whispering gallery modes through electron beam-induced deposition," Opt. Lett. **42**(7), 1337–1340 (2017).
16. F. J. Timmermans, B. Liszka, A. T. M. Lenferink, H. A. G. M. van Wolferen, and C. Otto, "Integration of correlative Raman microscopy in a dualbeam FIB SEM," J. Raman Spectrosc. **47**, 956–962 (2016).
17. V. Scheuer, H. Koops, and T. Tschudi, "Electron beam decomposition of carbonyls on silicon," Microelectron. Eng. **5**, 423–430 (1986).

#305665 https://doi.org/10.1364/OE.25.028946
Journal © 2017 Received 28 Aug 2017; revised 31 Oct 2017; accepted 31 Oct 2017; published 7 Nov 2017

Optics EXPRESS

1. Introduction

Whispering gallery modes (WGM) have been widely investigated for sensing [1, 2] and lasing [3, 4]. High quality factor WGM have also been used to study nonlinear properties of glass spheres [5]. A good theoretical understanding of the geometrical quantization of eigenmodes started with the pioneering work of Keller [6]. Comprehensive studies of geometrical and wave optics based theory provided a physical picture of Mie resonances [7, 8] and WGM [9–13]. Tsutaru *et al.* demonstrated a low threshold laser lasing in a 'non-WGM excitation' mode in a bubble-containing glass microsphere [4]. However, no explanation was proposed for the light path of their 'non-WGM excitation'. It was however remarked that excitation was different compared to that of "normal" WGM excitation. In this study, it is demonstrated that there are many more possibilities for resonating modes that can exist inside a microsphere, other than normal WGM, which propagate along the interface between a sphere or a disk and the surrounding medium. A relatively simple mathematical approach to find these modes will be explained on the basis of geometrical optics by ray tracing. Some of these possible modes are subsequently demonstrated experimentally. The understanding of these non-traditional WGM may lead to alternative design strategies for sensor applications or laser cavity configurations.

2. Geometrical mode calculation

Ioppolo *et al.* presented [13] a ray picture of a normal WGM, where the light was bouncing multiple times on the interface and back to its starting point after one round trip in a circle. The number of bounces was proposed to be very large in order to explain the conventional WGM, which propagates along the interface. However, as will be shown here, with a reduced number of reflections, many more resonating modes exist inside a sphere. Due to the law of reflection and the spherical geometry, all light rays are in a single plane which passes through the center of the sphere. Therefore, all the modes can be studied in a 2D circle. In this section, a method will be introduced to systematically calculate all possible geometrical modes in a circle. Additionally, a systematic label to these modes will be introduced first, as a way to individually distinguish these modes.

2.1 Nx2π-mode

Here the definition will be introduced of the Nx2π system to systematically refer to the modes and the definition will be explained with examples.

A resonating mode is a mode that overlaps with itself after certain distance of propagation. In a geometrical picture the light ray returns to an original location with the same direction. During light propagation, each reflection on the interface leads to a change in direction by angle θ_{change} in the propagation direction. The 'Nx2π' in the mode name describes the total propagation direction change when the light ray for the first time overlaps with itself.

The simplest example is a 1x2π-mode, where a light ray overlaps with itself after one round trip (thus $N = 1$) with J times reflections on the interface. The smallest J is 2 where the light ray passes through the center of the sphere and the angle $\theta_{change} = 180°$ for every reflection. In order to give an general explanation, an example of $J = 3$ is shown in Fig. 1. In this example, the light ray overlaps with itself for the first time after $J = 3$ reflections. The total propagation direction change is 360° (2π). Due to the circular geometry, every reflection has the same incident angle θ_i and change in propagation direction θ_{change}. Therefore, they can be calculated as:

$$\theta_{change} = \frac{360^{\circ}}{J}, \tag{1}$$

Optics EXPRESS

$$\theta_i = \frac{180^\circ - \theta_{change}}{2}. \quad (2)$$

If θ_i is smaller than the critical angle, then some light will refract out of the sphere with a refraction angle of θ_r. Otherwise, the light experiences total internal reflection. The length between adjacent reflection points is:

$$L_{br} = 2R\cos(\theta_i), \quad (3)$$

where R is the radius of the circle. The total optical path length of this mode is:

$$L_{op} = J \cdot L_{br} \cdot n_1, \quad (4)$$

where n_1 is the refractive index of the material of the sphere. This L_{op} is an approximation for the situation that L_{br} is much bigger than the wavelength λ. Thus the influence to the optical path length due to the phase delay at each reflection can be neglected.

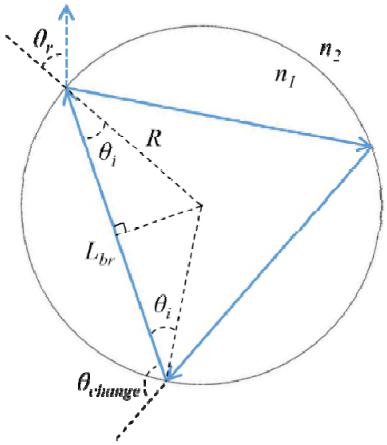

Fig. 1. Side view of the ray picture of the second 1x2π-mode. R is the radius of the circle. θ_i is the incident angle (the same as the reflection angle). L_{br} is the length between adjacent reflection points. θ_r is the refraction angle (in case of θ_i is smaller than the critical angle). θ_{change} is the change in propagation direction between reflections. n_1 and n_2 are the refractive index of the sphere and surrounding material respectively.

For a Nx2π-mode with the N bigger than 1, the light does not overlap with itself after 1 round trip inside the sphere, but after N times round trip. Therefore the total propagation direction changes is Nx360° (Nx2π). Thus, Eq. (1) will be written more generally as:

$$\theta_{change} = \frac{N \cdot 360^\circ}{J}, \quad (5)$$

With Eqs. (2)-(5), the optical path length of every mode becomes:

$$L_{op} = 2 \cdot J \cdot R \cdot n_1 \cdot \cos(90^\circ - \frac{N \cdot 180^\circ}{J}). \quad (6)$$

As J changes, there are multiple number of modes in a Nx2π-mode set. There are identical solutions with different N, J combination. For example, $N = 2$, $J = 6$ is the same mode as $N = 1$, $J = 3$. In order to address all the individual mode and exclude the degenerate ones, a number M is introduced to name the individual mode as N_M mode. M means the M^{th} unique mode in the Nx2π-modes, where the mode numbering starts with $N = 1$ in order of increasing J. The first few N_M modes are shown in Fig. 2 to demonstrate the mode characterization system.

Optics EXPRESS

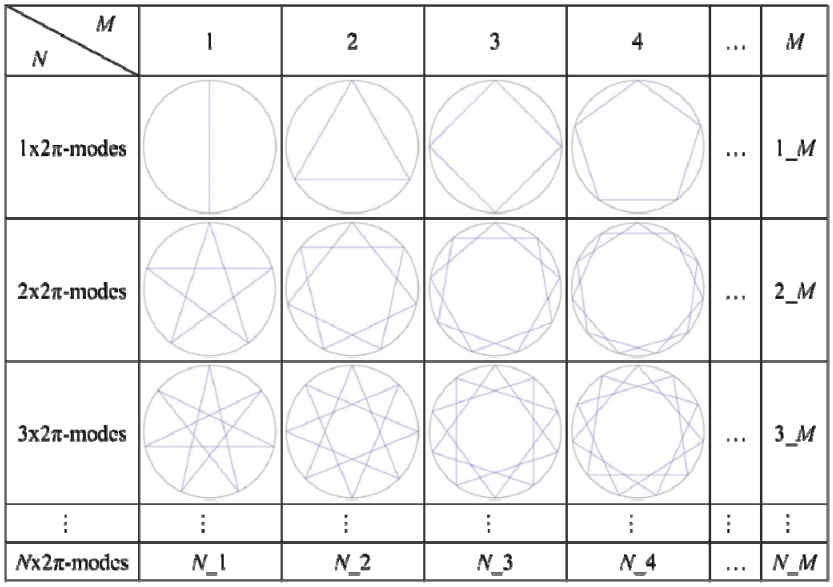

Fig. 2. Mode characterization system. The light paths (rays) of a few modes are shown (side view) as examples. *N* indicates the number of cycles before the light path overlaps with itself for the first time. Each *N* corresponds to a set of modes. Number *M* is used to identify every unique individual mode inside a given *N*x2π-mode set, in the order of an increasing number of reflections.

2.2 Mode detection principle

Spatial detection

Due to the center symmetry of a sphere, light emitted perpendicular to the sphere surface should be uniform everywhere on the surface. However, in the experimental situation (Fig. 3), an objective lens above the sphere is used to collect the light. In this way, a maximal detection efficiency occurs for the light propagating straight up.

For a mode with an incident angle θ_i smaller than the critical angle, light leaves the sphere mainly by refraction. The strongest detection of this mode should be at the location where the refracted light goes straight up. For example, the detected maximum from the top view should be at the center for the 1_1 mode (Fig. 2) and the detected maximum should be in between the center and edge for the 1_2 mode (Fig. 1).

For a mode with an incident angle θ_i equal to or larger than the critical angle, light leaves the sphere mainly by scattering at the surface. If it is assumed that the surface roughness is uniform and the scattered light intensity is the same in all directions, then the expected detection maximum is on the edge of the sphere in the top view. This is due to the fact that the pixels in the image are uniform in size and will, hence, collect from a larger surface area on the edge of the sphere than from the top of the sphere. In the other case, where it is assumed that the forward scattering from the surface is stronger than in any other direction, the expected detection maximal location is still on the edge of the sphere when viewed from the top. This is due to the fact that the light from the edge has a propagation direction that is directly into the opening angle of the objective. This means all the modes with an incident angle θ_i equal to or larger than the critical angle are expected to be detected on the edge of the sphere when viewed from the top.

Optical path length detection

Interference happens when the light ray overlaps with itself after one or more round trips. For a given mode, with optical path length of $L_{op}(N, M)$, certain wavelengths can fit integer

Optics EXPRESS

numbers and lead to constructive interference while others lead to destructive interference. This means a spectral intensity modification based on the L_{op} of a mode will occur. A Fourier analysis of the scattered light spectrum, which is commonly used in Fourier domain optical coherence tomography (OCT), can be used to identify the L_{op} of all the modes [14].

3. Experimental setup

3.1 Light source inside sphere

In order to better detect all possible modes inside a sphere, there are two requirements for the light source. First, a light source with a broad range of propagation directions inside the sphere is preferred, in order to excite as many modes as possible. Second, a light source with a smooth spectrum is preferred. Thus, any spectral modulation on top of the smooth spectrum is the result of interference of the modes with themselves after one or more round trips. Previously, WGM in micrometer-sized polystyrene spheres were visualized after electron beam induced deposition and subsequent laser irradiation to generate a local light source [15].

In the present experiments a different approach was chosen to generate a local light source. Two different light sources have been used namely thermal emission and Raman scattering inside a glass sphere. Both the thermal emission and Raman scattering are generated inside the glass sphere and propagate in all directions. The spectrum of the glass Raman scattering is not as smooth as that of thermal emission. However, the band of Raman scattering of glass is much wider than the modulation period caused by the mode interference of our large glass sphere. Therefore, the glass Raman spectrum is sufficiently smooth for our experimental condition. Thus, both these two light sources fulfill the two requirements mentioned above.

3.2 Equipment

The detection of the light scattering from modes in a sphere was performed with a confocal Raman micro spectrometer from Hybriscan Technologies B.V. integrated in a focused ion beam scanning electron microscope (FIB-SEM). The detection sensitivity of a Raman micro spectrometer system is advantageous to detect the low thermal light levels at the experimental temperature of ~580 °C. The integrated system enables correlative optical and electron microscopic analysis combined with focused ion beam sample modification on a correlated sample location. A mechanical stage is used to move the sample in between the FIB, SEM or optical microscope in the same vacuum chamber [16]. Figure 3(a) presents the experimental configuration, where the FIB (not shown) is behind the SEM end lens. The excitation laser in the Raman microscope has a wavelength of 785 nm and a maximal power of ~36 mW. The spectral detection range is from 806 nm to 988 nm. A more detailed description of the FIB-SEM-Raman system can be found in [16].

The electron beam is used to image the sample and locally deposit hydro-carbon material through a process known as electron beam induced deposition (EBID). The locally deposited hydro-carbon leads to an increase in light absorption and in this way increases the thermal emission by an increase of the emissivity, as predicted by Kirchhoff's law of thermal radiation. The FIB beam is used at low power and acts as an alternative way of hydro-carbon deposition.

The sample used in our experiment is soda-lime silica glass micro spheres (Sigma-Aldrich, 59200-U acid-washed). The glass spheres are heated to ~580 °C for a detectable thermal emission in our spectral detection range. The melting of the glass spheres (~600 °C) prevents a higher experimental temperature. The heating configuration is shown in Fig. 3(a) where the glass spheres are spread on top of a copper foil with low emissivity, to suppress thermal emission of the background. The copper foil is placed on top of a heater/sensor (Heraeus HD 421, Pt 100) with carbon paste (C-paste) in between the copper foil and the heater for better heat conductivity. A top view of the whole sample is shown with a SEM

Optics EXPRESS

image in Fig. 3(b). The thermal emission of a small drop of C-paste on top of the copper foil is used to acquire a better reading of the temperature on top of the copper foil.

3.3 Experimental procedure

One glass sphere, Figs. 3(c) and 3(d), is used as an example for all measurements discussed below. The glass sphere is heated to ~580 °C then the detection system of the confocal Raman microscope is used, with the Raman excitation laser off, to scan an area of 110 µm by 110 µm with a step size of 2 µm and the objective focused on the equatorial plane of the sphere. Due to the low thermal emission in the detected spectral range at this temperature, each spectrum is integrated for 10 seconds. The total scan time is ~10 hours for a 56 by 56 point image. In this way sufficient signal to noise ratio was obtained for the application of Fourier transform analysis.

One way to increase the light emission from the glass sphere without increasing the temperature is increasing the emissivity of the glass sphere. Based on Kirchhoff's law of thermal radiation, the emissivity increases with an increased absorption. In our experiment, the absorption was increased by EBID of hydro-carbon material on the glass sphere with SEM or FIB. The precise amount of deposition is unknown since it highly depends on the amount of hydro-carbon inside the vacuum chamber [17] and there is no quantitative control over the trace amounts. Therefore, all the depositions are only used qualitatively to indicate an increase in the total emissivity.

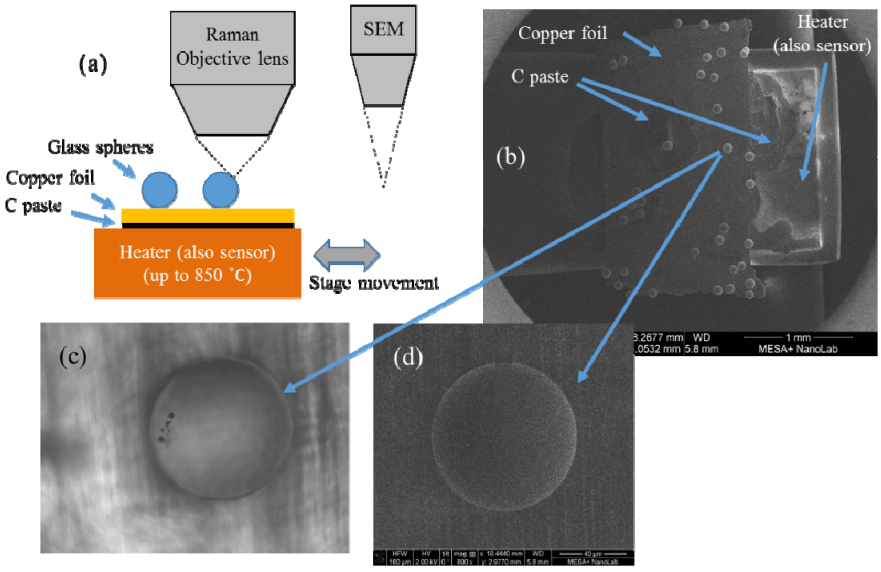

Fig. 3. Experimental setup and sample. (a) Figure of the setup and sample. The FIB head is behind the SEM end lens and not shown in this figure. The sample can be moved between FIB, SEM and Raman with a stage within the vacuum chamber. C paste is carbon paste. The C-paste in between the heater and copper foil is used to improve the heat conductivity. (b) Top view of the whole sample. (c) Optical image of the measured glass sphere, top view. (d) SEM image of the measured glass sphere, top view.

In order to further increase the light emitted inside the glass sphere, Raman scattering from the glass is added to the thermal emission in the last experiment. This is achieved by switching on the Raman excitation laser (36 mW) and maintaining the temperature of the glass sphere at ~580 °C.

Optics EXPRESS

4. Experimental results

4.1 Measured spectra and their Fourier transform (FT) plot

Examples of measured spectra are shown in Fig. 4(a). The FT spectra are shown in Fig. 4(b). In the FT spectra, a peak at an optical path length difference signifies constructive interference for those light paths. In our spherical sample, it means a mode interference with itself after one round trip. Therefore, a peak location in the FT plot is corresponding to the L_{op} of a mode.

The thermal spectrum example is measured at the center of the sphere (in the top view). At this location, only the 1_1 mode, round trip of two times of diameter, is expected. The optical path length, L_{op}, of this mode can be calculated by Eq. (6) with $N = 1$, $J = 2$, R and n_1. However, the R and n_1 of the sphere at the elevated temperature are not known precisely. Thus we calibrate the $R \cdot n_1 = 67.57$ μm with the measured L_{op} of the 1_1 mode. This number is then used to calculate the optical path length for all the other modes.

The Raman plus thermal spectrum example is measured on the edge of the sphere (in the top view). In principle, all the modes with an incident angle θ_i equal or larger than the critical angle (~41°) are expected. In practice, a limited number of modes are identified as shown in Fig. 4(b) as a result of the finite signal to noise ratio. Mode 2_2 and 3_4 have the incident angle θ_i of 38.6° and 40.9° respectively, which are smaller than the critical angle. Their expected detection maximum is very close to the edge of the sphere. Due to the finite mode size and limited spatial resolution, all the modes appear to emit from the edge. In this present work, we have only focused on the detection of modes and agreement with the proposed model. It is therefore relevant to know whether a mode exists or not and if it exists whether the mode has a peak at the predicted L_{op} location. The understanding of the peak height relation is planned for future work.

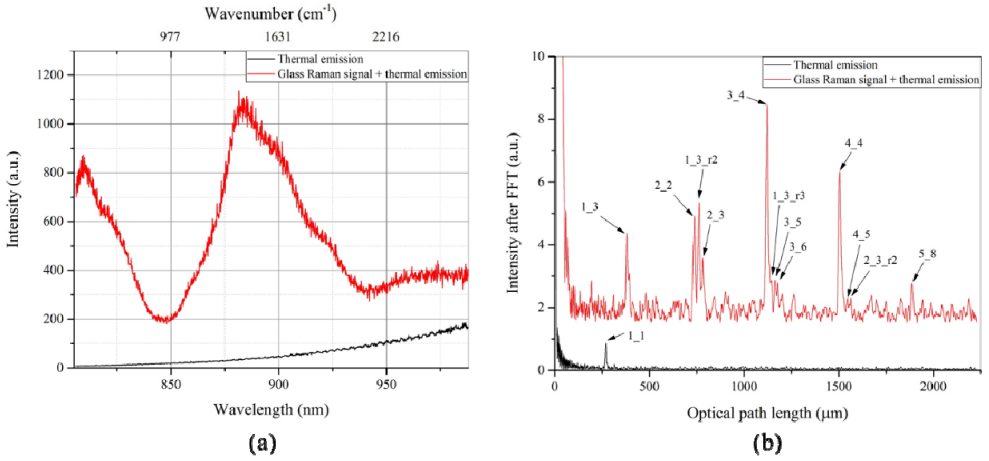

Fig. 4. (a) Example of measured thermal spectrum (black trace) and Raman + thermal spectrum (red trace) after carbon deposition by SEM and FIB operation. The thermal spectrum is measured at the center of the sphere. The Raman + thermal spectrum is measured on the edge of the sphere (in top view). The top relative wavenumber axis is used to help to read the glass Raman signal. (b) The Fourier transform of the spectra in (a). The identified modes are marked. Modes with suffix of '_r2' or '_r3′ are the same modes as the one without the suffix. The suffix is used to indicate the optical path length of 2 or 3 times of the L_{op}. This is caused by the light interference in that mode with itself after 2 or 3 times round trip.

Optics EXPRESS

Fig. 5. An overview of all 12 measured modes. The column at the extreme right has the name of the modes, their incident angle and the calculated and measured optical path length. Three modes with gray background are the modes detected also with multiple round trip. The second right column is the ray pictures (side view) of corresponding modes. The little arrows in mode 1_1, 1_2, 2_2 and 3_4 are used to indicate the location and direction of the detected refracted light. All the other images are the corresponding mode images (top view) constructed by integration over the L_{op} peak in the Fourier transform spectra of each mode at all scanned locations. The sphere is not perfectly round in the scanned top view. This is due to a small drift in the electron microscope scan stage during the long measurement time of ~10 hours.

Optics EXPRESS

4.2 Mode image and averaged FT plot over the mode area

The spatial distribution of a mode from the emission, a mode image, can be obtained by plotting the amplitude of the peak in the FT spectrum, corresponding to a certain mode number, at every location in the image. All the modes obtained in this experiment are shown in column 1-6 in Fig. 5. Column 7 is the ray pictures (side view) of corresponding modes. Column 8 presents the name of the mode, their incident angle and the calculated and measured optical path length. In practice, the mode image is very helpful to identify modes with a weak signal. For example, mode 4_5 is very difficult to discern in Fig. 4(b), however, by comparing the mode image at the L_{op} position and just beside it, a slightly brighter edge on the sphere can be recognized by eye at the L_{op} position for the 4_5 mode.

As the number of SEM or FIB depositions increases, the brightness of the local light field increases and the detectable number of modes also increases. This is due to the fact that an increase in thermal emission leads to a better signal to noise ratio, which subsequently helps with the mode identification.

In Fig. 5, column 6, it can be noted that a bright spot occurs close to the right-hand edge of the sphere in all mode images measured with the laser on. This spot should be ignored for the purpose of this study, as it results from a too high hydro-carbon deposition at that location during the second SEM deposition. This leads to an additional local temperature increase when the Raman laser is illuminating this location and hence the bright feature in the thermal emission spectrum.

All detected modes in this sample are located in the white area as shown in the insert of Fig. 6. By averaging all the FT spectra in this white area, an image of the FT spectra from all modes is obtained (the main plot of Fig. 6). The signal to noise ratio in this averaged FT plot is much better than the one in Fig. 4(b). Thus all the detected modes are more easily observed in this averaged FT plot. The difference in L_{op} between calculation and measurement is smaller than 0.2% for all modes.

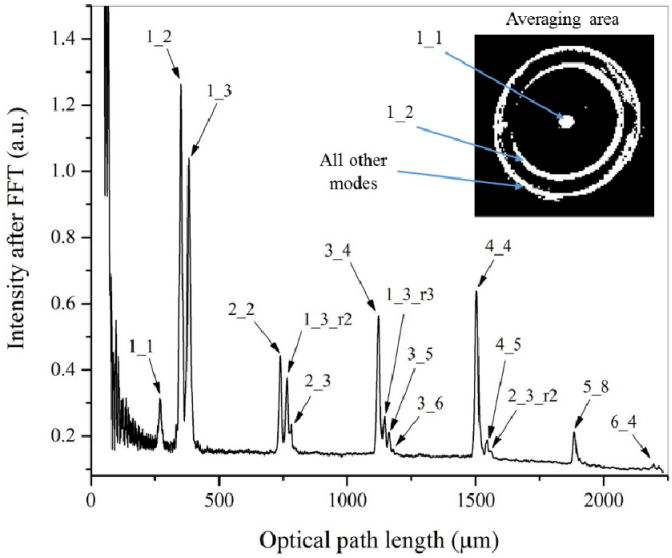

Fig. 6. Averaged FT spectra over the area of the detected modes. The insert is a binary top view image of all detected modes area. The 1_1 mode is located at the center. The 1_2 mode is located in between the center and the edge. All the other modes are located on or very close to the edge. The main plot is an average of all the FT plots in the white area of the inserted image.

Optics EXPRESS

4.3 Overview of the calculated and measured modes

An overview of all the calculated modes and measured modes in our sample are shown in Fig. 7. In order to generalize the figure to any sphere size and refractive index, a normalized round trip optical path length is used which considers $R{\cdot}n_1$ as unit one in Eq. (6). In this figure, the first N = 1, 2, …7 sets of Nx2π-modes are calculated as example. The most left-hand mode in each set has a M number M = 1. The M number increases in the same order as the incident angle θ_i. M approaches infinity when θ_i approaches 90°. The normalized round trip optical path length approaches to $N{\cdot}2\pi$ when θ_i approaches to 90°.

In our glass sphere sample, the critical angle and all the measured modes are marked in Fig. 7. There are only a few modes detected with θ_i smaller than the critical angle. This is due to the loss of refracted light at each reflection. There are more modes detected with θ_i bigger than the critical angle. However, at this moment, it is not fully understood why the detected FT intensity of these modes are different, which is the subject of ongoing research.

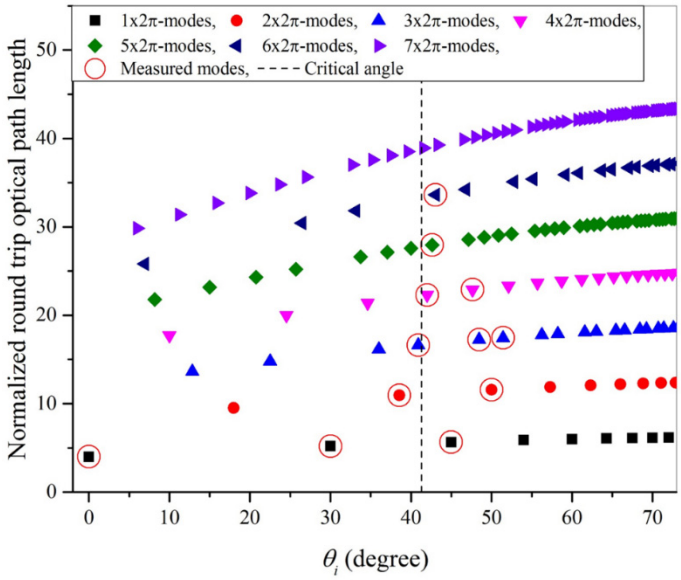

Fig. 7. Calculated normalized round trip optical path length as a function of incident angle for different modes. Normalized optical path length considers the $R{\cdot}n_1$ as unit one. Therefore, all the calculated modes can be universally applied to any spherical sample regardless the size and refractive index. All the modes measured in our sample are marked with a red circle. The dashed vertical line indicates the critical angle (~41°) in our sample.

5. Conclusions and suggestions

In this work, a systematic way was presented to calculate all possible ray modes inside a sphere or a circle. The normal WGM is one of the 1x2π-modes with θ_i close to 90°. By using the thermal emission and the Raman scattering from glass as an internal light source, it was possible to experimentally detect 12 different modes. All the detected modes have a measured optical path length, L_{op}, close to the predicted ones within 0.2% difference. Small differences may occur because the glass bead may not be a perfect, homogeneous sphere and the phase change during each reflection was not considered in our model. Similar results have been observed on several glass beads. The good correspondence of the theoretical prediction with the experimental observation is taken as evidence of the existence of these geometrical modes.

Now that the existence of these modes is proven, next steps to study the properties of these modes can be undertaken. Here, we propose three aspects which can be further studied. First, the beam size at every location along a mode path would deliver essential information

Optics EXPRESS

for the calculation of the coupling efficiency of an external or an internal light source to a certain mode.

Second, properties for different polarization states of the light field should be studied. For example, the modes with θ_i smaller than the critical angle are expected to be highly polarized due to the reflectivity difference at different polarization. On the other hand, the phase delay difference for different polarization will influence the modes with total internal reflections.

Third, it may be emphasized that the Q factor of each mode is important to know or compare with the normal WGM under the same condition. The potential applications of these modes may strongly depend on the Q factors of these modes. The variation in Q factor may also explain the peak height difference in the FT spectra in Fig. 6.

Here we propose two possible applications based on two known properties of the Nx2π-modes. First, the optical path length of a mode with $N > 1$ can be much larger than the optical path length of the circle (or sphere) perimeter. For example, the L_{op} of the mode 6_4 is 5.3 times larger than the perimeter. This means an effectively larger cavity can be realized by exciting a mode with larger N. This could be interesting for integrated optical devices, where a larger optical path length could be realized without increasing the physical size of a disk. Thus improving the integration density.

Second, sensing through one or a few modes could in principle extract the presence and distribution of the sensed subject, since each mode occupies a difference space inside the circle or the sphere.

Funding

De Nederlandse Organisatie voor Wetenschappelijk Onderzoek Toegepaste en Technische Wetenschappen (NWO-TTW) (12716).

Disclosures

C. Otto declares a potential conflict of interest as a managing director of the company HybriScan Technologies B.V. (www.hybriscan.com).